PERGAMON

Applied Radiation and Isotopes 54 (2001) 821–831

Applied Radiation and Isotopes

www.elsevier.com/locate/apradiso

Role of the activator in the performance of scintillators used in X-ray imaging

I. Kandarakis, D. Cavouras*

Department of Medical Instrumentation Technology, Technological Educational Institution of Athens, Ag. Spyridonos Street, Aigaleo, 122 10 Athens, Greece

Received 18 May 2000; received in revised form 1 August 2000; accepted 21 August 2000

Abstract

The aim of this study was to investigate how the activator type affects the performance of X-ray scintillators. To this aim the behavior of scintillator materials was modeled under X-ray excitation conditions, similar to those used in imaging techniques. The model describes the light emission efficiency, the spectral compatibility with optical detectors (films, photodiodes, and photocathodes), and the imaging capabilities of a scintillating layer. Using the model equations the role of the activator type in scintillator performance was examined. Activators affect some important properties of materials, like the intrinsic X-ray to light conversion efficiency, the spectrum of the emitted light, and the light attenuation coefficients. The performances of a high-efficiency material (Gd_2O_2S) combined with either Tb^{3+} or Eu^{3+} activators were compared. Results showed that the terbium-activated material exhibited high emission efficiency (number of emitted photons per incident X-ray) and modulation transfer function (spatial resolution and image contrast) while the europium activated material showed slightly better signal-to-noise ratio properties at low spatial frequencies. Both materials were found to exhibit high spectral compatibility with currently used modern optical detectors. In conclusion, the choice of activator may improve spectral compatibility, but care must be taken because it may also alter emission efficiency and image quality.

Keywords: Medical scintillators; Phosphor screens; Scintillator efficiency; MTF; DQE

1. Introduction

One of the most important properties of scintillation radiation detectors used in medical imaging systems, is the compatibility between the scintillator's light spectrum and the spectral sensitivity of the optical detector (photocathodes, photodiodes, CCDs, photographic-radiographic films, etc.). Poor spectral compatibility causes a decrease in the detector's sensitivity and image quality. In that case, in order to obtain high-quality results, the detector and, thus, the patient will have to be exposed to higher radiation doses. To improve spectral compatibility, activators may be employed during scintillator preparation, so that light spectra are modified to fit the sensitivity of existing optical detectors; Gd_2O_2S has been combined with Eu^{3+} activator in detectors using CCD arrays, and with Tb^{3+} activator in radiographic cassettes using orthochromatic films (Zweig and Zweig, 1983; Arnold, 1979; Curry et al., 1990; Gurwich, 1995; Gambaccini et al., 1996; Yaffe and Rowlands, 1997). CsI has been used with Tl when combined with silicon photodiodes and with Na when coupled to photocathodes (Mistretta, 1979; Haque and Stanley, 1981; Neitzel, 1997; Spahn et al.,1997; Yaffe and Rowlands, 1997). However, the type of activator may seriously affect the emission performance of the scintillator, a fact to which, to

*Corresponding address. 37-39 Esperidon Street, Kallithea 17671, Athens, Greece. Tel.: +301-5385-372/5385-375 (work)/ +301-9594-558 (home); fax: +301-5910-975 (work).

E-mail address: cavouras@hol.gr (D. Cavouras).

0969-8043/01/$ - see front matter
PII: S0969-8043(00)00336-5

our knowledge, little attention has been paid. The type of activator affects: (i) the intrinsic X-ray to light conversion efficiency (Tanaka et al., 1976; Alig and Bloom, 1977) and (ii) the attenuation (absorption and scattering) of light created within the scintillator material, by means of light wavelength shift (Van de Hulst, 1957; Gurwich, 1975; Arnold, 1979); light photons of shorter wavelengths are easier attenuated. Both these factors affect the intensity of the emitted light and the quality of the image produced.

In this work a theoretical model using experimental data was developed to study the role of the activator in the imaging performance of scintillators. The study is mainly concerned with the properties of granular scintillators; e.g. those employed in the form of layers containing scintillating grains. This type of detector is used in radiographic screens, in image intensifiers, in detectors of digital x-ray imaging systems, in portal imaging detectors used with linear accelarators, etc. (Arnold, 1979; Gurwich, 1995; Yaffe and Rowlands, 1997). Single-crystal scintillators, used in positron emission tomography or in single-photon emission computed tomography, differ from granular ones mainly in their intrinsic light scattering properties. The results of this work could also be interesting, however to a lesser extent, when considering the type of detectors with nongranular scintillators.

Scintillator performance was evaluated by the following parameters:

1. The detector optical gain (DOG), which expresses the emission efficiency of a scintillator by means of the number of emitted light photons per incident X-ray photon.
2. The modulation transfer function (MTF), which expresses image contrast and spatial resolution.
3. The detective quantum efficiency (DQE), expressing the output signal-to-noise ratio (SNR) with respect to the input signal-to-noise ratio.
4. The spectral matching factor, giving the compatibility between the spectrum of the emitted light and the spectral sensitivity of the optical detector.

The model was applied to a Gd_2O_2S scintillator, activated either with terbium (Tb^{3+}) or europium (Eu^{3+}) activators. Gd_2O_2S was chosen because it is a very efficient material characterized by: (a) high density ($7.44\,g/cm^3$), high effective atomic number (59.5), and, hence, high X-ray absorption efficiency in the energy range used in diagnostic imaging (Arnold, 1979; Zweig and Zweig, 1983; Gurwich, 1995) and (b) low semiconductor energy band gap resulting in high intrinsic X-ray-to-light conversion efficiency relative to other materials (Alig and Bloom, 1977; Gurwich, 1995; Kandarakis et al., 1997). Tb^{3+} and Eu^{3+} activators were considered since they are often used to produce light spectra in the "green" and "red" regions of the visible electromagnetic spectrum, respectively (Gurwich, 1995; Gambaccini et al., 1996; Cavouras et al., 1996; Cavouras et al., 1998a). Green or red lights are very useful in medical imaging, since they match very well to the spectral sensitivity of a large variety of optical detectors.

2. Materials and methods

In this study the following assumptions were made:

The scintillator has the form of a layer similar to the phosphor screens used in radiologic imaging or to the scintillating crystals of nuclear cameras.

The scintillator consists of phosphor grains embedded within a binding material.

X-ray absorption takes place only by the photoelectric effect.

X-rays fall perpendicularly to the detector surface.

2.1. Model description

The emission of light by an X-ray excited scintillator may be modelled as a four-stage process expressed by Eq. (1):

$$\bar{\Phi}_L(w_o) = \int_0^{E_{max}} \bar{\Phi}_X(E)\bar{\eta}_Q(E,w_o)\bar{m}_o(E)\int_0^{w_O} \bar{\varphi}_X(E,w) \times \bar{g}_L(\sigma,w)\,dw\,dE, \quad (1)$$

where $\bar{\Phi}_L(w_o)$ is the emitted light photon fluence representing the scintillator's output signal. w_o is the total coating thickness of the scintillator, often expressed as coating weight (mg/cm^2),$\bar{\Phi}_X(E)$ is the incident X-ray photon fluence averaged over the scintillator's area, $\bar{\Phi}_X$ is considered as the input signal and describes the first stage of the process corresponding to the X-ray incidence, E is the energy of an X-ray photon, $\bar{\eta}_Q$ is the average X-ray quantum detection efficiency (QDE), describing the second stage of X-ray absorption, $\bar{m}_0$ is the average number of light photons created within the scintillator per X-ray photon absorbed. This number expresses the third stage of the light emission process, which corresponds to the conversion of X-rays into light within the material.

The second integral in Eq. (1) expresses the transmission of light (from the point of light creation to the outer surface) through the scintillator material. This integral defines the light transmission efficiency corresponding to the fourth stage of the emission process. $\bar{g}_L(\sigma,w)$ is the average probability of a light photon, generated at depth w, to escape the scintillator (Swank, 1973) σ is a coefficient expressing the attenuation of light inside the scintillator and is defined as the reciprocal of the light diffusion length (Hamaker, 1947; Ludwig, 1971; Swank,

1973). $\bar{\varphi}_X$ is a function describing the relative distribution of X-ray absorption events at various depths w. For a given w, the value of $\bar{\varphi}_X$ gives the probability that an absorbed X-ray photon is absorbed at depth w (Swank, 1973; Van Metter and Rabbani, 1990; Kandarakis et al., 1999).

The first integral in Eq. (1) expresses the integration over the spectrum of the incident X-ray beam. E_{max} is the maximum energy of the spectrum. The second integral corresponds to the integration over the depth of X-ray penetration within the scintillator. The function $\bar{g}_L$ may be fourier-transformed and be represented in the spatial frequency domain, as a function of spatial frequency u (Swank, 1974; Dainty and Shaw, 1974; Nishikawa and Yaffe, 1990). The latter describes the frequency of periodic variation of a physical parameter in space (e.g. number of light photons in a unit of length). In the case of sinusoidal light variation, spatial frequency describes the number of maxima or minima per unit of length along an axis on the scintillator surface. Hence u is often expressed in cycles per cm. However, in X-ray imaging special patterns containing interlaced lead and transparent lines (line pairs) of varying widths, and hence of varying spatial frequencies, are used to experimentally evaluate spatial frequency dependent imaging parameters. Thus spatial frequency may be also expressed in line pairs per cm (lp/cm) (Dainty and Shaw, 1974; Curry et al., 1990, Cavouras et al., 2000); it can be easily conceived that large objects (few variations per unit length) in an image contribute to the low-frequency image content while small objects (many variations per unit length) correspond to high frequencies. From Eq. (1), it is shown that the emitted light fluence, may be also represented in the spatial frequency domain as a function of spatial frequency $\bar{\Phi}_L(u, w_o)$.

An additional factor that must be considered in Eq. (1) is the spectral matching factor (Giakoumakis, 1991; Cavouras et al., 1998a). The latter describes the spectral compatibility between the emitted light and the spectral sensitivity of the optical detector. Using this factor, the effective light photon fluence may be defined as follows:

$$\bar{\Phi}_{L,eff}(u, w_o) = \bar{\Phi}_L(u, w_o) c_\lambda \tag{2}$$

where c_λ is the spectral matching factor defined by the equation

$$c_\lambda = \int_{\Delta\lambda} \varphi_L(\lambda) S_D(\lambda)\, d\lambda \Big/ \int_{\Delta\lambda} S_D(\lambda)\, d\lambda, \tag{3}$$

where $\varphi_L(\lambda)$ is the normalized spectrum of the emitted light, $S_D(\lambda)$ is the spectral sensitivity distribution function of the optical detector. λ denotes light wavelength and $\Delta\lambda$ is the bandwidth of the emitted light spectrum.

Using the definition of $\bar{\Phi}_L$ in terms of spatial frequency u, two parameters evaluating scintillator performance, the gain transfer function (GTF)- G_P, and the modulation transfer function (MTF)- M_P, may be defined as follows (Swank, 1973; Van Metter and Rabbani, 1990; Van Metter, 1992; Cavouras et al., 2000):

$$G_P(u, w_o) = \frac{\bar{\Phi}_L(u, w_o)}{\bar{\Phi}_X(E_o)}, \tag{4}$$

$$M_P(u, w_o) = \frac{\bar{\Phi}_L(u, w_o)}{\bar{\Phi}_L(0, w_o)}, \tag{5}$$

where $\bar{\Phi}_X(E_o)$ denotes the integral of $\bar{\Phi}_X(E)$ over the X-ray spectrum and expresses the incident X-ray photon fluence (input signal). Eq. (4) gives the number of emitted light photons (NEP) per incident X-ray photon at various spatial frequencies. Each spatial frequency value corresponds to a certain size of the object to be imaged, through which X-rays are transmitted before entering the scintillator. At zero spatial frequency $u = 0$, GTF may be defined as the detector optical gain (DOG), expressed as the number of emitted photons per incident photon. This is equivalent to the luminescence emission efficiency (Ludwig, 1971; Swank, 1973; Kandarakis et al., 1998; Kandarakis et al., 1999), which determines the brightness of the final image for a given level of X- ray exposure.

Eq. (5) gives the spatial-frequency-dependent output signal normalized to the zero-frequency signal. It expresses the fraction of output signal corresponding to each spatial frequency value. MTF is used to describe image contrast and spatial resolution. MTF may also be found by fourier transforming the point spread function (PSF). This function describes the spread of output light, originating from a point source within the scintillator.

Both MTF and GTF are parameters related to the scintillator's output signal. However, the detection efficiency of a scintillator and the quality of the output image, are largely affected by the presence of quantum noise. The latter may be expressed by the statistical variance in $\bar{\Phi}_L$ (Shaw and Van Metter, 1984; Yaffe and Rowlands, 1997; Cavouras et al., 1998b). To determine this variance, the fractional variances of Φ_X, η_Q, m_o, g_L must be calculated and added (Shaw and Van Metter, 1984; Cavouras et al., 1998b; Cavouras et al., 2000). If the result of the calculations is fourier transformed, then the quantum noise may be expressed in the fourier domain, as a function of spatial frequency, by the noise amplitude spectrum (NAS)- N_P or the noise power spectrum (NPS)- W_P. NPS, which is also referred to as Wiener spectrum, may be calculated by the following relation (Shaw and Van Metter, 1984; Nishikawa and Yaffe, 1990; Van Metter and Rabbani, 1990; Cavouras

et al., 1998b; Cavouras et al., 2000):

$$W_P(u,w_o)=\int_0^{E_{max}}\bar{\Phi}_X(E)\bar{\eta}_Q(E,w_o)[\bar{m}_o(E)]^2\times\int_0^{w_0}[\bar{\varphi}_X(E,w)\bar{g}_L(u,\sigma,w)]^2\,dw\,dE+\int_0^{E_{max}}\bar{\Phi}_X(E)\bar{\eta}_Q(E,w_o)\bar{m}_o(E)\times\int_0^{wO}\bar{\varphi}_X(E,w)\bar{g}_L(0,\sigma,w)\,dw\,dE. \quad (6)$$

It must be noted that Eq. (6) holds only in the case where m_0 follows Poisson statistics, which is a reasonable assumption (Shaw and Van Metter, 1984; Nishikawa and Yaffe, 1990).

The overall performance of a scintillator may be described by the signal-to-noise ratio (SNR). The latter is often expressed by the detective quantum efficiency (DQE)-η_D, defined as follows (Dainty and Shaw, 1974; Shaw and Van Metter, 1984):

$$\eta_D(u,w_o)=\frac{[SNR_o(u,w_o)]^2}{SNR_I^2}, \quad (7)$$

where SNR_o is the output signal-to-noise ratio and SNR_I is the input signal-to-noise ratio. Taking into account Eqs. (1), (4), (5), the output signal-to-noise ratio may be written as

$$SNR_o^2(u,w_o)=\frac{[\bar{\Phi}_L(u,w_o)]^2}{[N_P(u,w_o)]^2}=\frac{[\bar{\Phi}_L(u,w_o)]^2}{W_P(u,w_o)}=\frac{[G_P(u,w_O)\bar{\Phi}_X(E_o)]^2}{W_P(u,w_o)}, \quad (8)$$

where we have considered that $N_P^2=W_P$.

The input signal-to-noise ratio may be determined by considering that the incident X-ray photons follow Poisson statistics. The signal-to-noise ratio may be written as the ratio of the mean value of Φ_X over the variance of Φ_X (Shaw and Van Metter, 1984; Cavouras et al., 1998b; Cavouras et al., 2000). However, in Poisson statistics, the variance is equal to square root of the mean value of Φ_X. Hence, the input signal to noise ratio may be written as

$$SNR_I^2=\bar{\Phi}_X(E_o). \quad (9)$$

Thus, the detective quantum efficiency may be written as

$$\eta_D(u,w_o)=\frac{[\bar{\Phi}_L(u,w_o)]^2}{\bar{\Phi}_X(E_o)W_P(u,w_o)}=\frac{[\bar{\Phi}_X(E_o)G_P(u,w_o)]^2}{\bar{\Phi}_X(E_o)W_P(u,w_o)}=\frac{[\bar{\Phi}_L(0,w_o)M_P(u,w_o)]^2}{\bar{\Phi}_X(E_o)W_P(u,w_o)}. \quad (10)$$

Since DQE describes output signal in the presence of noise, it expresses the complete imaging capability of a scintillator and quantifies the overall information content in the final image. Additionally DQE has been found to be the parameter of most importance for detectors of modern digital imaging systems (Moy, 2000).

2.2. Calculations

To determine $\bar{\Phi}_L, G_P, M_P, W_P, \eta_D, a_S$ the functions $\bar{\Phi}_X$, $\bar{\eta}_Q, \bar{m}_o, \bar{\varphi}_X, \bar{g}_L, \varphi_L, S_D$ describing the four stages of the X-ray excitation and light emission process were determined as follows:

1. $\bar{\Phi}_X$ was calculated using previously published theoretical models (Tucker et al., 1991) describing the spectral distribution of the incident X-ray photon fluence. The maximum energy E_{max} of the X-ray spectrum was set equal to 30 keV. Additionally, the spectrum was considered to be produced by a molybdenum anode X-ray tube and filtered by an additional 0.5 cm filter of aluminum, to simulate attenuation by human tissue (breast).

2. $\bar{\eta}_Q(E,w_o)$was calculated considering exponential X-ray absorption governed by the X-ray absorption coefficient and the thickness of the scintillator. Absorption coefficients were calculated using data on Gd, O and S from published tables (Storm and Israel, 1967).

3. $\bar{m}_o(E)$was calculated by the equation

$$\bar{m}_o(E)=\eta_C E/(hc/\lambda), \quad (11)$$

where, $\eta_C$is the intrinsic X-ray to light conversion efficiency of the scintillator expressing the fraction of absorbed X-ray energy converted into light within the scintillator. The denominator in Eq. (11) expresses the energy of a light photon. Values for $\eta_C$were obtained as follows: For Gd_2O_2S: Tb η_C was taken from our previous experimental studies (Kandarakis et al., 1997) on this material where, using fitting techniques, it had been found equal to 0.20. For Gd_2O_2S:Eu, $\eta_C$was taken equal to 0.12. This value was selected by taking into account: (a) The value $\eta_C=0.11$ given by (Alig and Bloom, 1977) for cathodo-luminescence excitation conditions, (b) previous studies that have shown η_C to be slightly higher under X-ray excitation than under cathodo-luminescence conditions (De Poorter and Bril, 1975; Cavouras et al., 1996; Kandarakis et al.,1997). For the wavelength λ we have used mean values $\bar{\lambda}$, determined from our previous measurements on Gd_2O_2S:Tb spectrum and from published data on Gd_2O_2S:Eu (Gambaccini et al, 1996), as follows:

$$\bar{\lambda}=\int_{\Delta\lambda}\varphi_L(\lambda)\lambda\,d\lambda/\int_{\Delta\lambda}\varphi_L(\lambda)\,d\lambda, \quad (12)$$

where $\varphi_L(\lambda)$ is the spectrum of the phosphor. The values found were 545 nm for Gd_2O_2S:Tb and 626 nm for Gd_2O_2S:Eu.

4. For the function $\bar{g}_L(\sigma,w)$ we have used the solution of a photon diffusion differential equation (Swank,

1973), in the presence of a light scattering medium (see the appendix).

The value of the light attenuation coefficient σ for Gd_2O_2S: Tb, was taken from previous studies where, using fitting techniques to experimental data (Press et al., 1990), it was found equal to $30\,cm^2/g$. For Gd_2O_2S:Eu the value of σ was estimated by considering the following: (a) light attenuation is mainly due to scattering because of the granular form of the scintillator, (b) the size distribution of the grains in the two scintillators is the same which, according to the data sheets of a phosphor powder manufacturer (Lumilux, Riedel de Haen, Germany), has an average value of $7\,\mu m$, (c) It has been previously theoretically shown (Lindström and Carlsson, 1999) that the calculated scintillator efficiency remains practically unaltered if we consider that it consists of identical grains of size equal to the average size of the real scintillator grains, and (d) since the average size of the grains is larger than light wavelength, the scattering coefficient is approximately proportional to λ^{-2} (Van de Hulst, 1957). Thus σ was set equal to $23\,cm^2/g$.

5. The function $\bar{\varphi}_X(E,w)$ was expressed by the equation

$$\bar{\varphi}_X(E,w)=\frac{\mu(E)\exp[-\mu(E)w]\,dw}{\int_0^{w_0}\mu(E)\exp[-\mu(E)w]\,dw}, \tag{13}$$

where $\mu(E)$is the X-ray absorption coefficient calculated as described above for the detection efficiency $\bar{\eta}_Q$. The numerator in Eq. (13) gives the probability of X-ray photon absorption at depth w. The denominator is equal to the total probability of absorption in a scintillator of thickness w_0.

6. The spectral matching factor c_S was calculated using scintillators' emission spectra and data on spectral sensitivity of optical detectors from manufacturers' data.

3. Results and discussion

Fig. 1 shows the zero-frequency gain transfer function $G_P(0,w)$ of Gd_2O_2S:Tb and Gd_2O_2S:Tb scintillators, determined for five coating weight values, ranging from 20 to $45\,mg/cm^2$. This range of coating weights corresponds to the phosphor screen thicknesses often used in X-ray mammography. The maximum energy of the X-ray spectrum was 30 keV, which corresponds to a voltage often employed in mammography. Two curves are presented for each phosphor, one corresponding to the light emitted by the scintillator surface receiving the X-ray beam (reflection mode), and one corresponding to the light emitted by the non-irradiated side of the screen (transmission mode). Reflection mode simulates light emission from the rear side of a conventional radiographic cassette or from mammographic cassettes, while transmission mode simulates all other types of imaging radiation detectors (front screen of radiographic cassettes, image intensifier input screens, computed tomography detectors, gamma camera, etc.). As it is observed the gain is higher in reflection mode. This difference

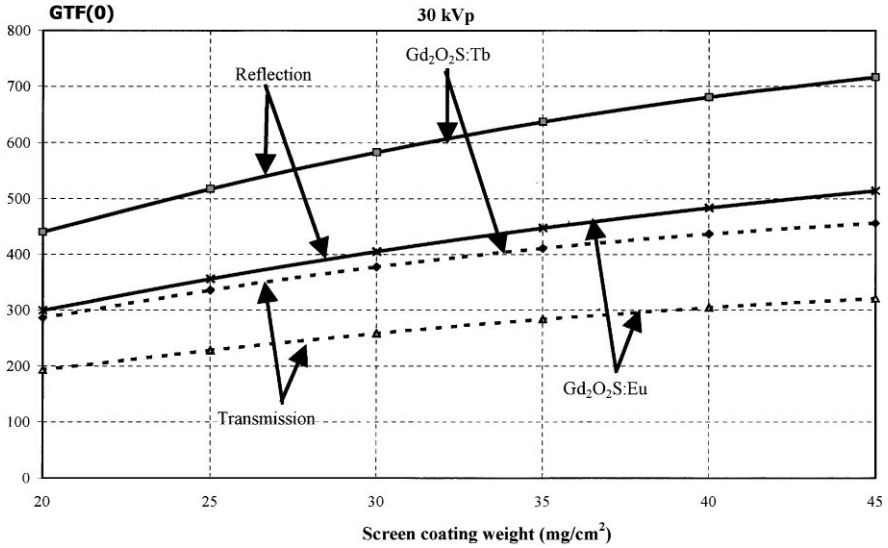

Fig. 1. Variation of the zero-frequency gain transfer function (emitted light photons/incident X-ray photon) of Gd_2O_2S:Tb and Gd_2O_2S:Eu scintillators, with increasing coating weight, determined in transmission and reflection mode at 30 kVp (approximately 18 keV average X-ray energy).

between the two modes is due to the exponential variation of the X-ray absorption and light transmission with scintillator thickness, and is explained as follows: (i) function $\bar{\varphi}_X$, describing the distribution of absorbed photons in Eq. (1), decreases with increasing X-ray penetration depth w and, hence, $\bar{\varphi}_X$ takes higher values close to the irradiated surface. (ii) $\bar{g}_L(\sigma, w)$, describing the probability of light photon escape, decreases with screen thickness and, thus, it attains higher values for those light photons generated at depth w and directed towards the irradiated surface, since they travel shorter distances to escape relative to those photons traveling in the opposite direction. It can be also observed from Fig. 1 that the gain transfer function increases with increasing coating weight in both modes. This results from the exponential increase of the X-ray quantum detection efficiency, $\bar{\eta}_Q(E, w_o)$, with increasing total scintillator thickness. Fig. 1 also shows the variation of the transmission mode GTF($u = 0$) with coating weight for both Gd_2O_2S:Tb and Gd_2O_2S:Eu. The terbium-activated scintillator was found to exhibit approximately 30% higher light emission performance than the europium activated one. This may be explained as follows: both materials have equal X-ray absorption coefficients and hence the respective $\bar{\eta}_Q$and $\bar{\varphi}_X$ functions are identical. The value of the light attenuation coefficient σ is lower for Gd_2O_2S:Eu, giving higher values for the function $\bar{g}_L$. However, the superior emission efficiency of Gd_2O_2S:Tb is due to its significantly higher intrinsic conversion efficiency η_C (0.20 instead of 0.12 for Gd_2O_2S:Eu).

Figs. 2–4 show the results obtained for the modulation transfer function $M_P(u, w_o)$ of the scintillators. In Fig. 2 MTF curves corresponding to various coating weights are presented displaying the decrease of MTF with increasing scintillator thickness. This is in contrast to the behavior of GTF(0) with increasing thickness, indicating that a compromise between image brightness and image quality should be made in practical applications.

Fig. 3 compares transmission and reflection mode MTFs. The higher values obtained in reflection mode may be explained in a similar way as in the case of GTF(0). Physically, this means that more X-ray photons are absorbed at depths closer to the irradiated surface. Hence, light photons created at the same depth have to penetrate shorter distances when directed towards the irradiated side. This is equivalent to what is intuitively accepted for the point spread function of thin phosphor screens. In thin screens, light spread is restricted within a limited scintillator area. This corresponds to narrow PSF curves which, after fourier transforming result in high MTF curves.

Fig. 4 shows a comparison between the MTFs of Gd_2O_2S:Tb and Gd_2O_2S:Eu for scintillator layers of 35 mg/cm^2. Since the intrinsic conversion efficiency, $\bar{\eta}_C$, appears in both the numerator and denominator in Eq. (5), the principal factor determining the slight MTF difference between both materials is the optical attenuation coefficient σ. This may be physically explained by considering that if the light attenuation coefficient is higher, as in the case of Gd_2O_2S:Tb, the laterally directed light photons, which travel longer distances to arrive at the scintillator surface, are highly attenuated. Thus, light spread at the output surface is limited within a small area. This reduces the width of the point spread

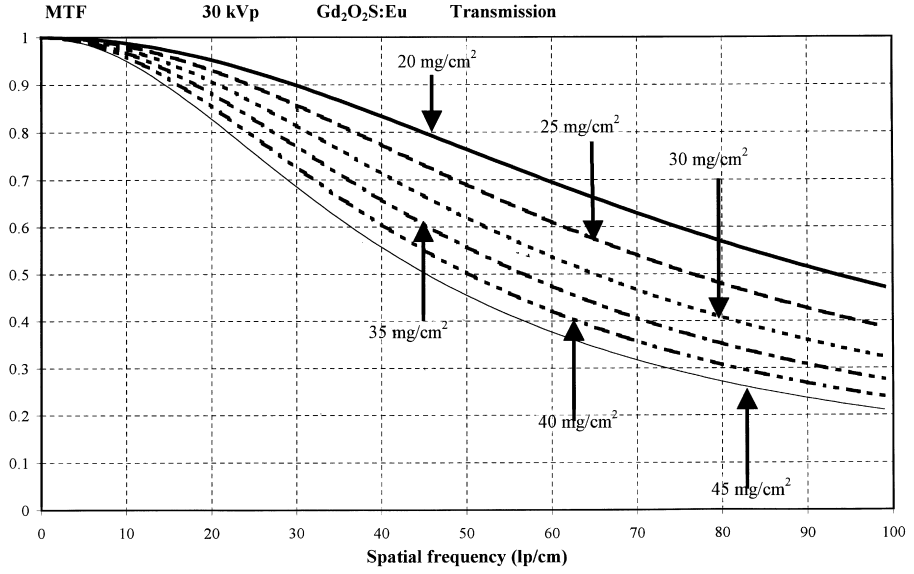

Fig. 2. Modulation transfer function of Gd_2O_2S:Eu scintillator for various coating weights, determined in transmission mode.

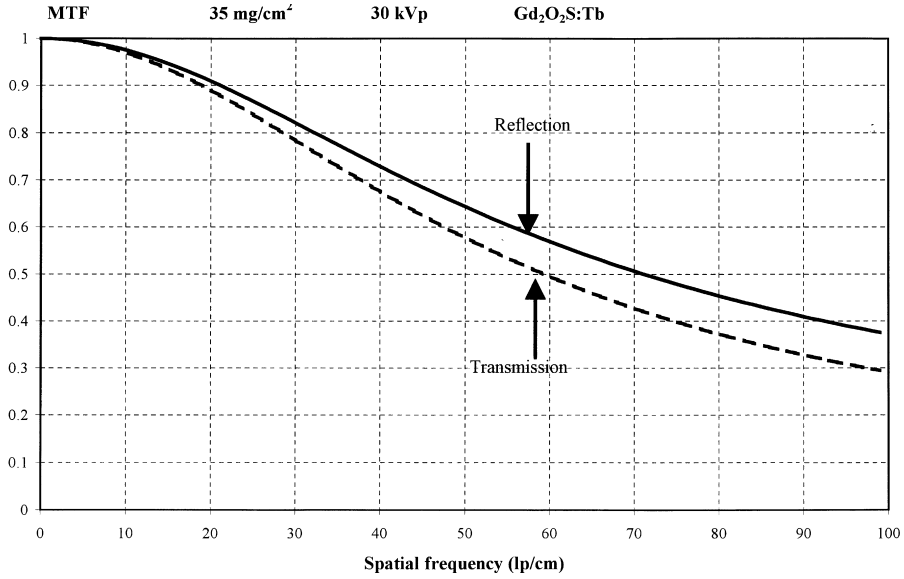

Fig. 3. Modulation transfer function of the 35 mg/cm^2 Gd_2O_2S:Tb scintillator layer in reflection and transmission mode.

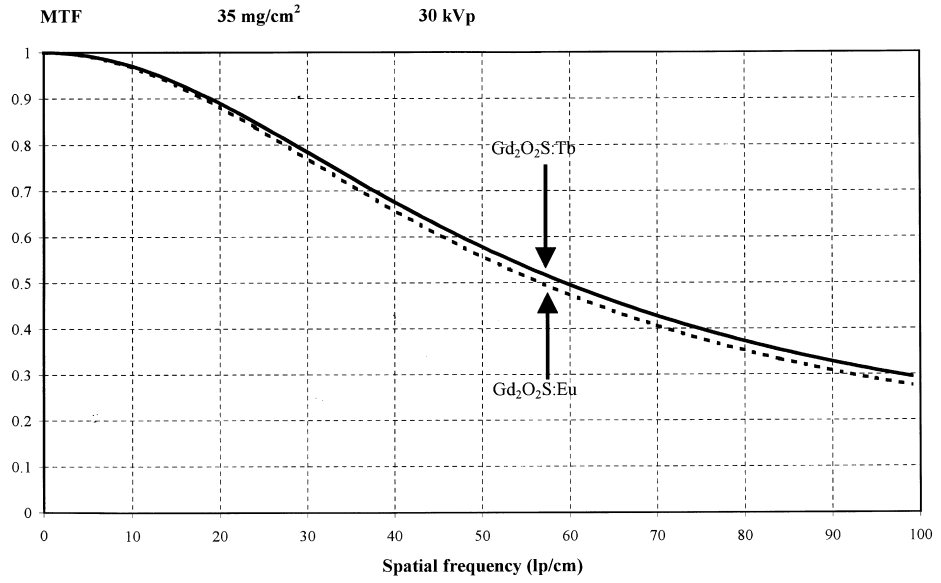

Fig. 4. Comparison of the modulation transfer functions of Gd_2O_2S:Tb and Gd_2O_2S:Eu scintillators determined in transmission mode.

function resulting, after fourier transform, in higher MTF values for Gd_2O_2S:Tb.

Figs. 5 and 6 show results obtained for the spatial-frequency-dependent DQE. All data shown correspond to transmission mode since the differences between both modes were found insignificant. Fig. 5 is a plot of DQE for various coating weights. At the low spatial frequency range, DQE increases with coating weight showing a variation similar to that of GTF(0). This is in accordance with the definition of DQE in Eq. (10). However, the thicker the scintillator layer the higher the rate of DQE decreases with spatial frequency. Thus, at high frequencies thin layers exhibit higher DQE than thick layers. This type of variation is due to a

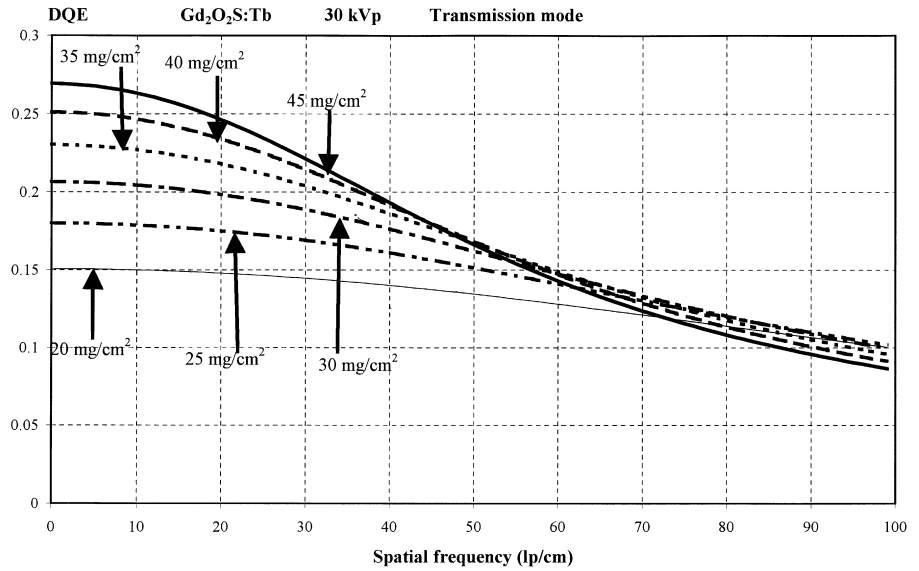

Fig. 5. Detective quantum efficiency of Gd_2O_2S:Tb scintillator for various coating weights, determined in transmission mode.

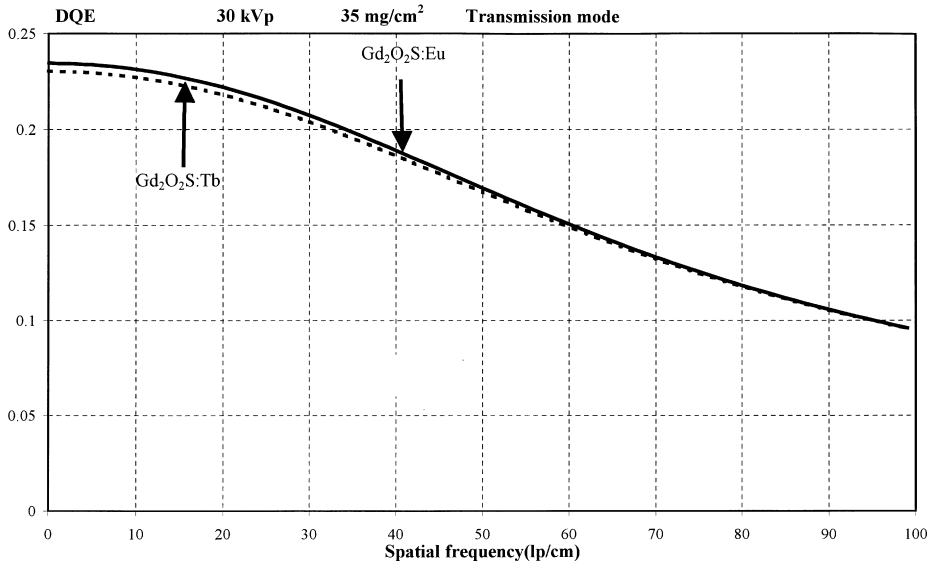

Fig. 6. Comparison of the detective quantum efficiencies of Gd_2O_2S:Tb and Gd_2O_2S:Eu scintillators, determined in transmission mode.

corresponding variation in MTF (see Eq. (10)), which increases with decreasing coating weight.

A comparison between the DQEs of Gd_2O_2S:Tb and Gd_2O_2S:Eu is shown in Fig. 6. The two curves are very close. The DQE of Gd_2O_2S: Eu slightly exceeds the DQE of Gd_2O_2S: Tb at the low-frequency range. DQE is not significantly affected by the intrinsic conversion efficiency η_C, since this parameter appears in both numerator and denominator of Eq. (10). Thus, differences between both materials are mainly due to the different values of the light attenuation coefficient σ. Low values of σ increase the zero-frequency signal $\bar{\Phi}_L(0, w)$ and, hence, SNR and DQE are affected in a similar way. This may explain the slight superiority of Gd_2O_2S:Eu ($\sigma = 23\,cm^2/g$) over Gd_2O_2S:Tb ($\sigma = 30\,cm^2/g$) in the low-frequency range. As frequency increases, the role of MTF, which increases with σ, becomes more evident. This has a slight effect on the

Table 1
Spectral matching factors

Scintillator	c- Si photodiode	a-Si photodiode	S 20 Photocathode	Film
Gd_2O_2S: Tb	0.54	0.92	0.78	0.69[a]
Gd_2O_2S: Eu	0.68	0.77	0.59	0.91[b]

[a] Orthochromatic film.
[b] Film sensitive to red light.

DQE of Gd_2O_2S:Tb and, thus, both curves coincide for frequencies higher than 40 lp/cm. Since DQE is an important parameter expressing the overall performance of a scintillator, both materials, although different in GTF(0), may be considered of equivalent imaging capabilities.

All results presented in this study concerning MTF and DQE, are within the limits of or, in some cases, higher to published experimental data obtained on commercial X-ray imaging detectors (Bunch et al., 1987; Nishikawa and Yaffe, 1988, 1990; Van Metter and Rabbani, 1990; Beutel and Kitts, 1996; Williams et al., 1999; Vedantham et al., 2000; Moy, 2000). Discrepancies between published experimental data and our results may be mainly attributed to the fact that most of these data refer to integrated detector systems (e.g. scintillators coupled to optical detectors like films or photodiodes, etc.) and not to single scintillator layers. Additionally discrepancies may also be attributed to differences in intrinsic material properties (e.g. grain size, chemical processing with special light absorbing dyes, higher or lower light reflectivities due to different binding materials, etc.).

Table 1 shows the calculated values of the spectral matching factor for combinations of Gd_2O_2S:Tb and Gd_2O_2S:Eu with four optical detectors, namely: (a) crystalline silicon (c-Si), used in photodiodes or CCD arrays of computed tomography or digital radiography detectors, (b) amorphous silicon (a-Si), used in detectors of flat panel digital radiography systems and in some computed tomography detectors (Haque and Stanley, 1981; Neitzel, 1997; Spahn et al., 1997), (c) extended sensitivity S20 photocathode (E/S 20), used in image intensifiers of conventional or digital fluoroscopy and in photo-multipliers in nuclear medicine gamma cameras, and (d) radiographic films of 'green' or 'red' sensitivity, used in conventional radiographic cassettes (Arnold, 1979; Curry et al., 1990). As it is observed, Gd_2O_2S:Eu shows higher spectral compatibility with c-Si than Gd_2O_2S:Tb and with Agfa Scopix LT2B film than Gd_2O_2S:Tb with the corresponding Agfa Curix ortho GS orthochromatic film. On the other hand Gd_2O_2S: Tb is better with a-Si. This is very interesting, since a-Si is employed in some very modern imaging applications. Of course Gd_2O_2S: Tb is very well matched to the Agfa Curix ortho GS film, currently employed in conventional radiography. Hence, both materials may be used in various modern imaging modalities depending on the spectral sensitivity of the corresponding optical detector.

4. Summary and conclusion

A model describing the performance of scintillator materials for use in radiation detectors of imaging systems was described. The model predicts the gain transfer function, the modulation transfer function, the detective quantum efficiency and the spectral compatibility with optical detectors. Using this model, the role of the activator type in the overall scintillator performance was examined by comparing Gd_2O_2S:Tb and Gd_2O_2S:Eu scintillators. The different activator modifies the intinsic X-ray to light conversion efficiency, the light emission spectrum and the optical attenuation coefficient. These modifications have the following consequences on scintillator performance: The terbium-activated material was found to exhibit better output gain (emitted photons per incident X-ray) and modulation transfer function while the europium-activated scintillator was found with slightly higher detective quantum efficiency at low spatial frequencies. Both materials were found with satisfactory spectral compatibility with modern optical detectors sensitive to red or green light. Thus, the choice of activator may improve spectral compatibility with a specific type of optical detector, but it may also significantly influence emission efficiency and image quality.

Acknowledgements

This study is dedicated to the memory of Prof. G.E. Giakoumakis, leading member of our team, whose work on phosphor materials has inspired us to continue.

Appendix

The function $\bar{g}_L(u, w)$ has been defined as a solution to a photon diffusion differential equation (Swank, 1973),

which describes the propagation of light through light scattering media, and it is given as follows:

$$\bar{g}_{\mathrm{L}}(u,w)=\frac{\rho_1[(\beta+\rho_0)\mathrm{e}^{\sigma w}+(\beta-\rho_0)\mathrm{e}^{-\sigma w}]}{(\beta+\rho_0)(\beta+\rho_1)\mathrm{e}^{\sigma w_0}-(\beta-\rho_0)(\beta-\rho_1)\mathrm{e}^{-\sigma w_0}}, \tag{A.1}$$

where σ is the light attenuation coefficient of the scintillator, which is equal to the reciprocal of the light photon diffusion length (Hamaker, 1947; Ludwig, 1971; Swank, 1973) and it is given as a function of the optical scattering coefficient, s, and the optical absorption coefficient, a,:

$$\sigma=[a(a+2s)]^{1/2}. \tag{A.2}$$

In the spatial frequency domain, σ is written as (Swank, 1973):$\sigma=\sigma_0^2+4\pi u^2$ where $\sigma_0$is the zero-frequency light attenuation coefficient.

ρ_0,ρ_1 are optical parameters expressing the reflection of light at the front and back scintillator surfaces defined as

$$\rho_{\mathrm{n}}=(1-r_n)/(1+r_n),\quad n=0,1, \tag{A.3}$$

where r_n denotes the optical reflection coefficients at the front (0) and back (1) screen surfaces.

β is an optical parameter which is equal to ρ, corresponding to the case of a very thick scintillator with no light transmission.β has been also expressed as a function of a and s (Ludwig, 1971):

$$\beta=[a/(a+2s)]^{1/2}. \tag{A.4}$$

Previous measurements (Cavouras et al., 1996; Kandarakis et al., 1997; Kandarakis et al., 1999) have shown that β and ρ_{n} had the same value for a large number of scintillating materials: $\beta=0.03,\rho_0=0.91,\rho_1=0.87$. These values were also used for both materials in this study. Eq. (A.1) corresponds to transmission mode. To describe reflection mode emission w, in Eq. (A.1) should be simply replaced by w_0–w.

References

Alig, R.C., Bloom, S., 1977. Cathodoluminescent efficiency. J. Electrochem. Soc. 124, 1136.

Arnold, B.A., 1979. Physical characteristics of screen-film combinations In: Haus, A.G. (Ed.), The Physics of Medical Imaging: Recording System, Measurements and Techniques. American Association of Physicists in Medicine, New York, pp. 30–71.

Beutel, J., Kitts, E.L., 1996. The image quality characteristics of a novel film/screen system for mammography. Proc. SPIE. 2708, 233.

Bunch, P.C., Huff, K.E., Van Metter, R., 1987. Analysis of the detective quantum efficiency of a screen-film system. J. Opt. Soc. Am. A4, 902.

Cavouras, D., Kandarakis, I., Panayiotakis, G., Evangelou, E.K., Nomicos, C.D., 1996. An evaluation of the $Y_2O_3:Eu^{3+}$ scintillator for application in medical X-ray detectors and image receptors. Med. Phys. 23, 1965.

Cavouras, D., Kandarakis, I., Bakas, A., Triantis, D., Nomicos, C.D., Panayiotakis, G.S., 1998a. An experimental method to determine the effective luminescence efficiency of scintillator - photodetector combinations used in X-ray medical imaging systems. Br. J. Radiol. 71, 766.

Cavouras, D., Kandarakis, I., Kanellopoulos, E., Nomicos, C.D., Panayiotakis, G.S., 1998b. Signal to noise ratio (SNR) of X-ray imaging scintillators determined by luminescence measurements. Appl. Radiate Isot. 51, 59.

Cavouras, D., Kandarakis, I., Nomicos, C.D., Panayiotakis, G.S., 2000. Assessing the information content of phosphor-produced medical images application to $Zn_2SiO_4:Mn$ phosphor. Appl. Radiate Isot. 52, 119.

Curry, T.S., Dowdey, J.E., Murry, R.C., 1990. Luminescent screens, the radiographic image. In: Lea, Febiger (Ed.,) Christensen's Physics of Diagnostic Radiology. London, pp.118–136, 196–218.

Dainty, J.C., Shaw, R., 1974. Detective quantum efficiency signal to noise ratio and the noise-equivalent number of quanta. In: Image science. Academic Press, New York, pp. 152–188.

De Poorter, J.A., Bril, A., 1975. Absolute X-ray efficiencies of some phosphors. J. Electrochem. Soc. 122, 1086.

Gambaccini, M., Taibi, A., Del Guerra, A., Marziani, M., Tuffanelli, 1996. MTF evaluation of a phosphor coated CCD for X-ray imaging. Phys. Med. Biol. 41, 2799.

Giakoumakis, G.E., 1991. Matching factors for various light-source-photodetector combinations. Appl. Phys. A52, 7.

Gurwich, A.M., 1995. Luminescent screens for mammography. Radiat. Meas. 24, 325.

Hamaker, H., 1947. Radiation and heat conduction in light-scattering material. Philips Res. Rep. 2, 55.

Haque, P., Stanley, J.H., 1981. Basic principles of computed-tomography detectors. In: Newton, T.H., Potts, D.G. (Eds.), Radiology of the Skull and Brain Technical Aspects of Computed Tomography. C.V. Mosby Company, St. Louis, 4103 pp.

Kandarakis, I., Cavouras, D., Kanellopoulos, E., Nomicos, C.D., Panayiotakis, G.S., 1998. Experimental determination of detector gain, zero frequency detective quantum efficiency, and spectral compatibility of phosphor screens: comparison of $CsI:Na$ and $Gd_2O_2S:Tb$ for medical imaging applications. Nucl. Instr. and Meth. A 417, 86.

Kandarakis, I., Cavouras, D., Panayiotakis, G.S., Nomicos, C.D., 1997. Evaluating X-ray detectors for radiographic applications: a comparison of $ZnSCdS:Ag$ with $Gd_2O_2S:Tb$ and $Y_2O_2S:Tb$ screens. Phys. Med. Biol. 42, 1351.

Kandarakis, I., Cavouras, D., Prassopoulos, P., Kanellopoulos, E., Nomicos, C.D., Panayiotakis, G.S., 1999. Evaluating $Zn_2SiO_4:Mn$ phosphor for use in medical imaging radiation detectors. Appl. Phys. A 67, 521.

Lindström, J., Carlsson, G.A., 1999. A simple model for estimating the particle size dependence of absolute efficiency of fluorescent screens. Phys. Med. Biol. 44, 1353.

Ludwig, G.W., 1971. X-ray efficiency of powder phosphors. J. Electrochem. Soc. 118, 1152.

Mistretta, C.A., 1979. X-ray image intensifiers. In: Haus, A.G. (Ed.), The Physics of Medical Imaging Recording System

Measurements and Techniques. American Association of Physicists in Medicine, New York, pp. 182–205.

Moy, J.P., 2000. Signal-to-noise ratio and spatial resolution in X-ray electronic imagers: is the MTF a relevant parameter?. Med. Phys. 27, 86.

Neitzel, U., 1997. Integrated digital radiography with a flat electronic detector. Medicamundi. 41, 14.

Nishikawa, R.M., Yaffe, M.J., 1988. Modelling the spatial-frequency-dependent detective quantum efficiency of X-ray image receptors. Proc. SPIE 914, 128.

Nishikawa, R.M., Yaffe, M.J., 1990. Model of the spatial-frequency-dependent detective quantum efficiency of phosphor screens. Med. Phys. 17, 894.

Press, W.H., Flannery, B.P., Teukolsky, S.A., Vetterling, W.T., 1990. In: Numerical Recipes in C: The Art of Scientific Computing. Cambridge University Press, Cambridge, pp. 540–547.

Shaw, R., Van Metter, R., 1984. An analysis of the fundamental limitations of screen-film systems for X-ray detection. Proc. SPIE 454, 128.

Spahn, M., Alexander, J., Gmeinwieser, J., 1997. Amorphous silicon solid- state detectors and their future applications in medical X-ray imaging. Electromedica 65, 37.

Storm, E., Israel H., 1967. Photon cross-sections from 0.001 to 100 MeV for elements 1 through 100. *Report LA-3753*, Los Alamos Scientific Laboratory, University of California.

Swank, R.K., 1973. Calculation of modulation transfer functions of X-ray fluorescent screens. Appl. Opt. 12, 1865.

Tanaka, S., Maruyama, Y., Kobayashi, H., Sasakura, H., 1976. Electroluminescence in rare earth doped Y_2O_3,La_2O_3, and Y_2O_2S powder layers. J. Electrochem. Soc. 123, 1917.

Tucker, D.M., Barnes, G.T., Wu, X., 1991. Molybdenum target X – ray spectra: a semiempirical model. Med. Phys. 18, 402.

Van de Hulst, H.C., 1957. In: Light Scattering by Small Particles. Wiley, New York, pp. 103–107.

Van Metter, R., 1992. Describing the signal-transfer characteristics of asymmetrical radiographic screen-film systems. Med. Phys. 19, 53.

Van Metter, R., Rabbani, M., 1990. An application of multivariate moment-generating functions to the analysis of signal and noise propagation in radiographic screen-film systems. Med. Phys. 17, 65.

Vedantham, S., Karellas, A., et al., 2000. Full breast digital mammography with an amorphous silicon-based flat panel detector: physical characteristics of a clinical prototype. Med. Phys. 27, 558.

Williams, M.B., Simoni, P.U., Smillowitz, L., Stanton, M., Philips, W., Stewart, A., 1999. Analysis of the detective quantum efficiency of a developmental detector for digital mammography. Med. Phys. 26, 2273.

Yaffe, M.J., Rowlands, J.K., 1997. X-ray detectors for digital radiography. Phys. Med. Biol. 42, 1.

Zweig, G., Zweig, D.A., 1983. Radioluminescent imaging: factors affecting total light output. Proc SPIE. 419, 297.